FTIR Spectral Components of Schwertmannite

Jean-François Boily[1,§], Paul L. Gassman[2], Tetyana Peretyazhko[2], János Szanyi[2] and John M. Zachara[2]

[1] Department of Chemistry, Umeå University, Umeå SE-901 87, Sweden
[2] Pacific Northwest National Laboratory, Richland, WA 99352, USA

§ corresponding author.:   email: jean-francois.boily@chem.umu.se
                              phone: +46 90 786 5270

Table S1. Cross-peaks from asynchronous 2D-CS maps of Figs. 2 b & c

pH 3.0-4.4 (Fig 2b)

	cm^{-1}	b 1180	c 1160	e 1120	g 1070	h 1033	i 990	j 972	k 960
b	1180		▓		▓				
c	1160	▓		▓		▓			░
e	1120		▓		▓		░		
g	1070	▓		▓		▓			
h	1033		▓		▓			░	░
i	990								░
j	972		░			░			
k	960		░			░	░		

pH 4.4-9.0 (Fig. 2c)

	cm^{-1}	a 1210	c 1160	d 1130	f 1108	h 1033	i 990	j 972	k 960
a	1210		▓		▓			░	
c	1160	▓		▓		▓	░		░
d	1130		▓		▓				
f	1108	▓		▓		▓	░		░
h	1030		▓		▓				
i	990	░	░	░				░	
j	972						░		
k	960		░		░				

Note. Shaded areas denote presence of cross-peaks. Lighter shaded squares denote cross-peaks involving ν_1 modes. White area denote possible correlation between bands. Those involving ν_1 modes are less reliable due to their small intensities.
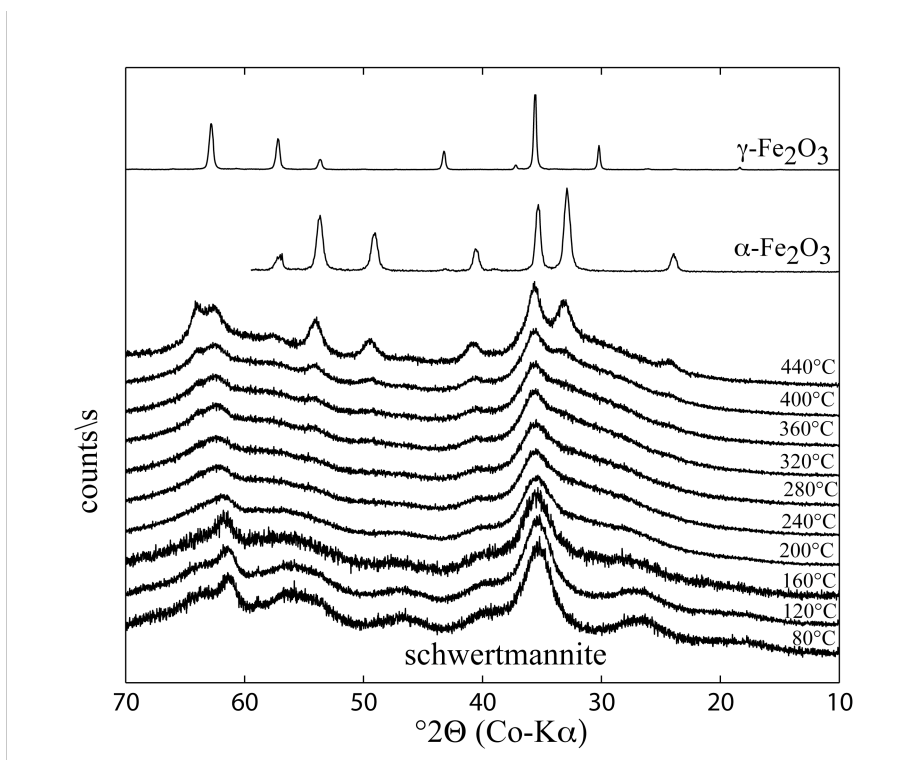
Figure S1. X-ray diffractograms of synthetic schwertmannite reacted to 440°C for 4h under atmospheric conditions. Diffractograms of crystalline hematite and maghemite samples are shown for comparison.
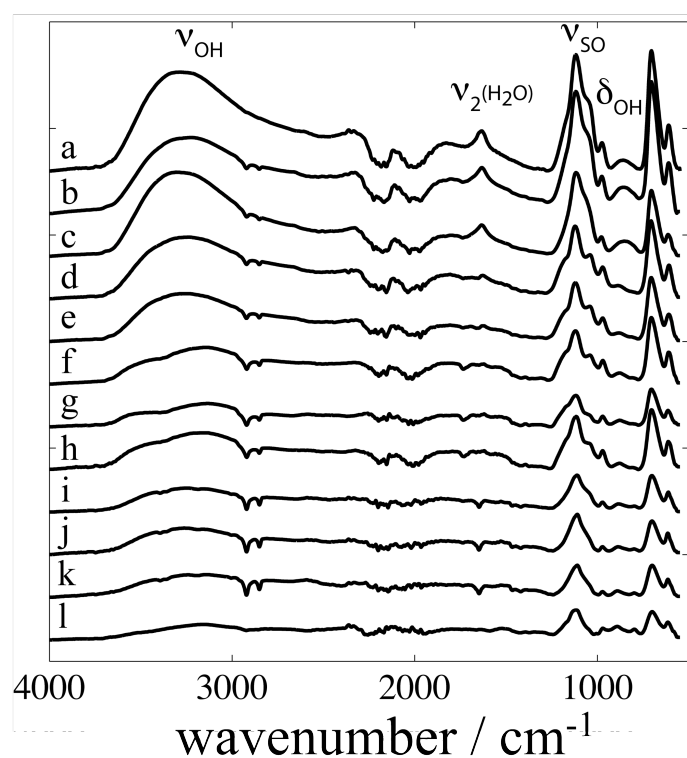

Figure S2. ATR-FTIR spectra of synthetic schwertmannite filtered and dried from suspensions at pH values of 3.14 (a), 3.44 (b), 4.00 (c), 4.40 (d), 5.05 (e), 5.50 (f), 6.13 (g), 6.52 (h), 6.65 (i), 8.04 (j), 8.44 (k) 9.04 (l) at 298.2 K.
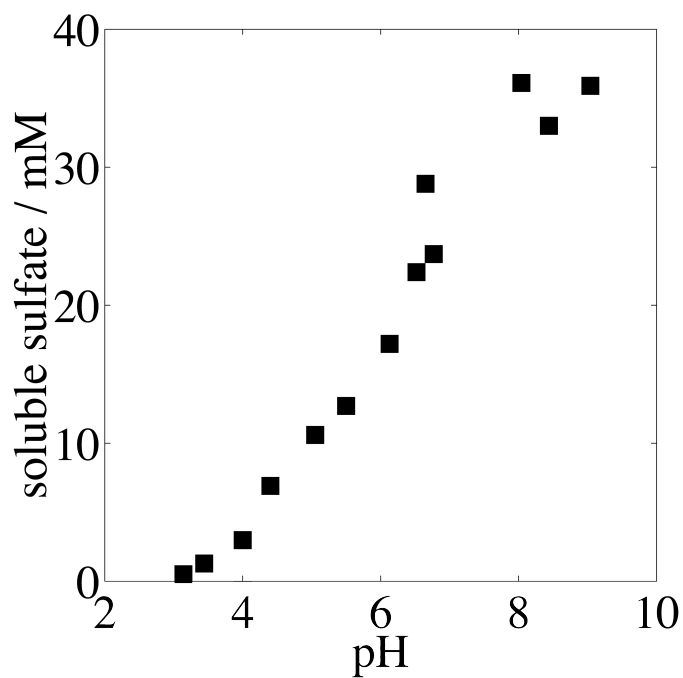
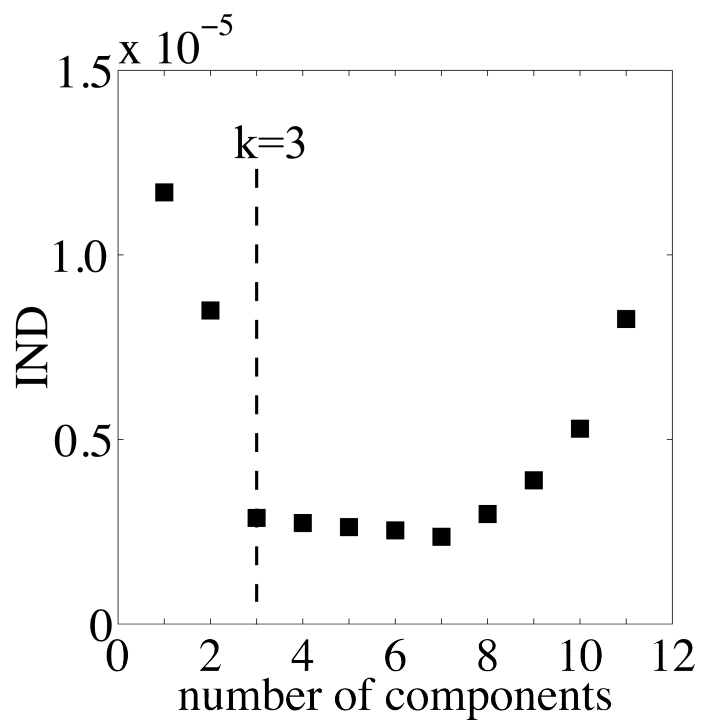**Figure S3.** Soluble sulfate concentration of the solids (50.0 g/L) reacted at different pH values.

Figure S4. IND values from S-O stretching region of Fig. 1. The spectra can be reproduced with 3 linearly-independent factors.
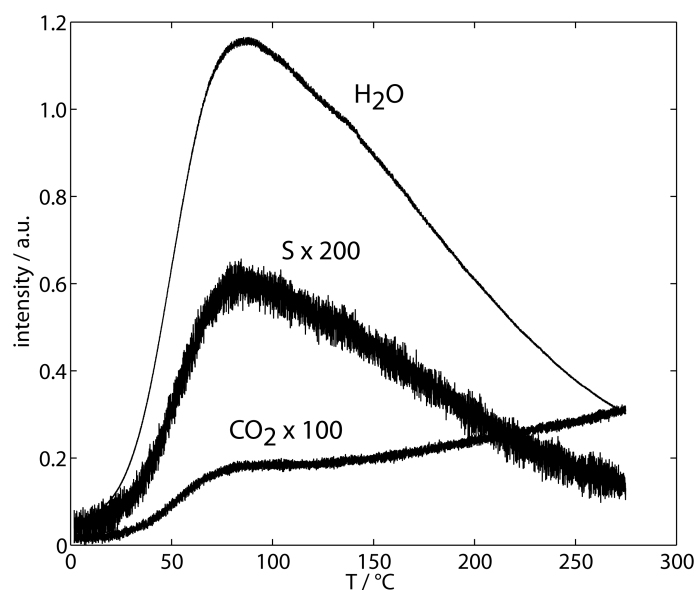
Figure S5. Mass spectrometric analyses of evolved gases by TPD. The detected mass-to-charge (*m/e*) values corresponded to H_2O (*m/e*=18), S (*m/e*=32) and CO_2 (*m/e*=44). Cracking fragments of H_2O and CO_2 were also detected (not shown) and followed a congruent TPD trace with the parent molecule. The released sulfur arises from weakly-bound hydrate sulfate ions, given the similarily between the S and H_2O TPD traces. A small amount of entrapped carbonate, similar to findings of Bigham *et al.* [17], follows a similar decarbonation pattern to goethite-carbonate solid solutions [29]. The amount of carbonate present is below the detection limits of the infrared spectrometers and is therefore of no consequence to this study.
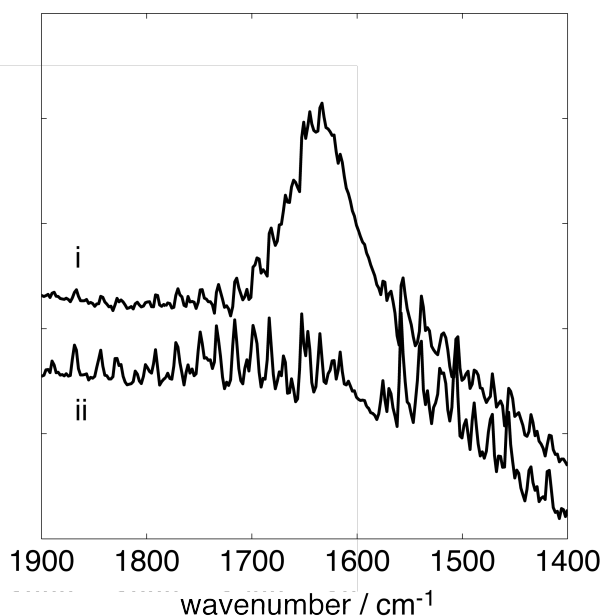
Figure S6. MCR components of the water bending region of synthetic schwertmannite in $N_2(g)$ in the 30-130°C range. Component i and ii belong to the same sets as those for the O-H and S-O stretching regions (Fig. 4c-d). Their pH concentration profiles are show in Fig. S7. The multiple sharp peaks are from gaseous water molecules whose contributions were not subtracted from the data. Note that component ii contains no water and therefore only represents the baseline of this region.
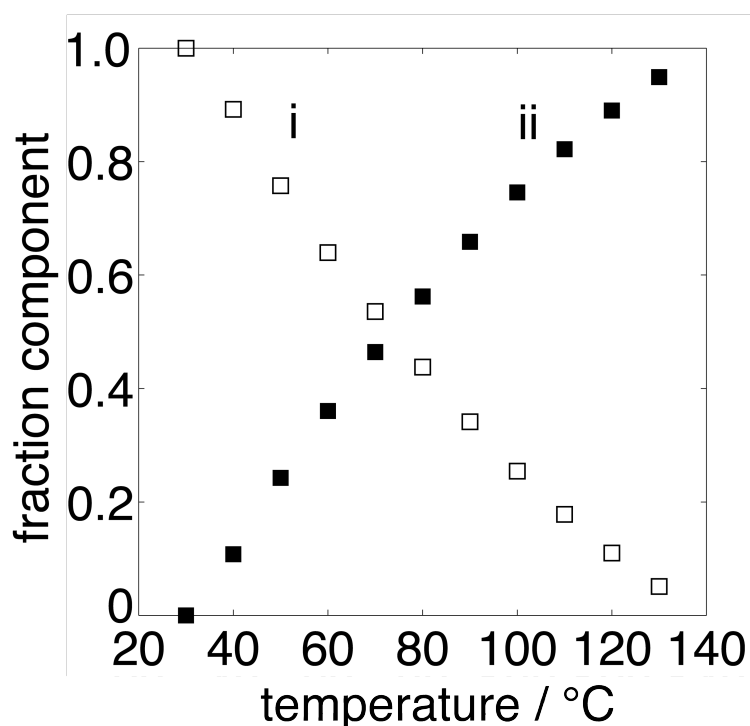

Figure S7. Fractions of components i and ii of synthetic schwertmannite in the 30-130°C range. Component i and ii belong to the same sets as those for the S-O stretching (Fig. 4c), water stretching (Fig. 4d) and the water bending (Fig S7) regions.
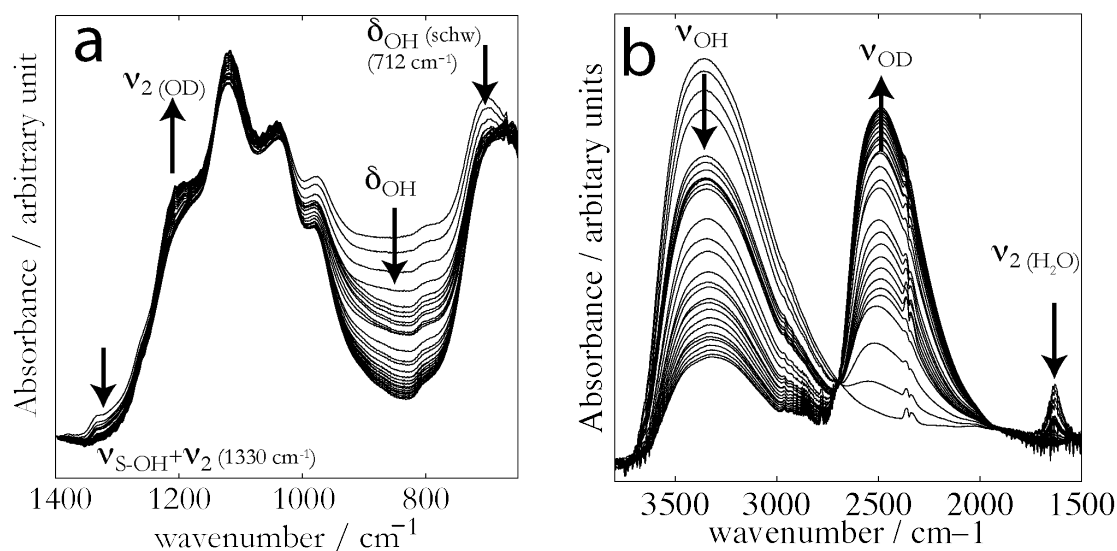
Figure S8. Microscopic FTIR spectra of a synthetic schwertmannite powder heated at 130°C for 4h and reacted to a saturated atmosphere of D_2O vapor in $N_2(g)$. The arrows denote the direction of spectral change for the (a) the ν_1 and δ_{OH} and (b) ν_{OH} modes. The 1330 cm^{-1} $\nu_{S-OH}+\nu_2$ combination band is readily affected, confirming that it may arise from a protonated sulfate group. The 712 cm^{-1} band is assigned to a OH deformation in schwertmannite for (OH$\cdots$O-SO$_3$) and is also readily affected by deuteration. The isotopic shift of the broad 860 cm^{-1} OH deformation to this region however affects the intensities.